Supplementary Information

Modulator-free approach towards missing-cluster defect formation in Zr-based UiO-66

Patchanee Chammingkwan,[a] Goji Yildun Shangkum,[a,b] Le Thi Tuyet Mai,[a] Priyank Mohan,[a] Ashutosh Thakur,[a] Toru Wada[a] and Toshiaki Taniike*[a]

[a]Graduate School of Advanced Science and Technology, Japan Advanced Institute of Science and Technology, 1-1 Asahidai, Nomi, Ishikawa, 923-1292 Japan.
[b]Department of Chemistry, Faculty of Natural Sciences, University of Jos, P.M.B 2084, Jos Plateau State, Nigeria.

*E-mail: taniike@jaist.ac.jp.

Characterizations

1. X-ray diffraction

The crystalline structure of UiO-66, UiO-66-CH$_3$ and UiO-66-NH$_2$ was analyzed by X-ray diffraction (XRD, Rigaku SmartLab) using Cu Kα radiation in the range of 2θ = 5-45° at the step of 0.1° per 150 s.
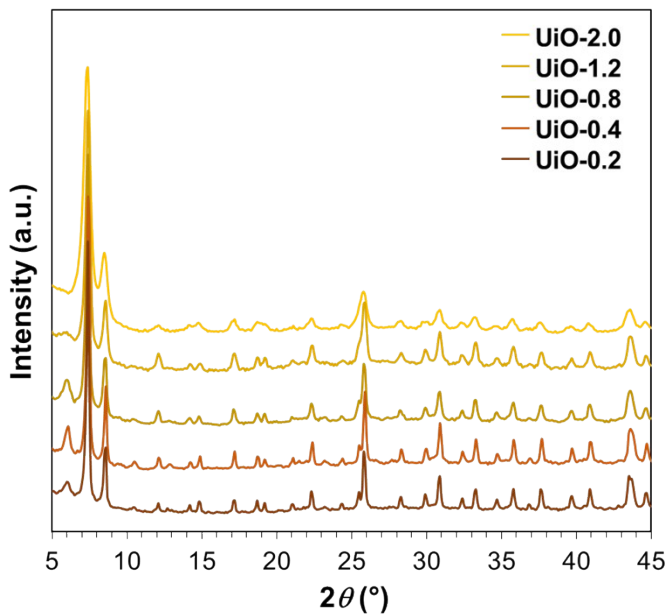
Fig. S1 XRD patterns of UiO-66 samples in the range of 5-45°.
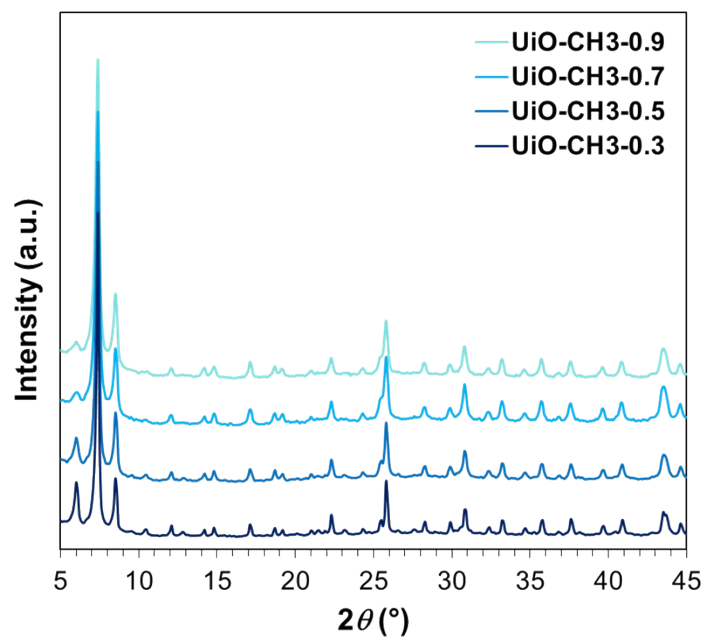
Fig. S2 XRD patterns of UiO-66-CH$_3$ samples in the range of 5-45°.
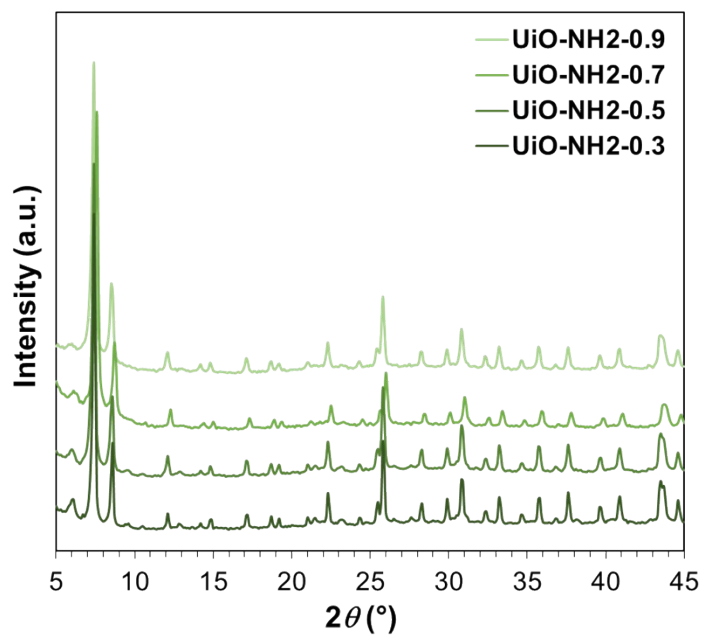
Fig. S3 XRD patterns of UiO-66-NH$_2$ samples in the range of 5-45°.

2. Transmission electron microscopy

The morphology of UiO-66, UiO-66-CH$_3$ and UiO-66-NH$_2$ was observed using transmission electron microscopy (TEM, Hitachi H7100) at an accelerated voltage of 100 kV. A dried sample was dispersed in methanol, deposited onto a copper grid by drop casting, and then dried under air to evaporate the solvent. The particle size was acquired based on the TEM image analysis using the ImageJ software.
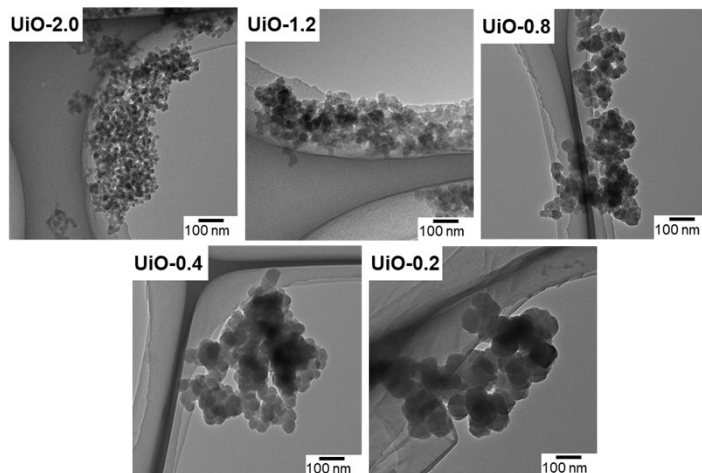
Fig. S4 TEM images of UiO-66 samples.
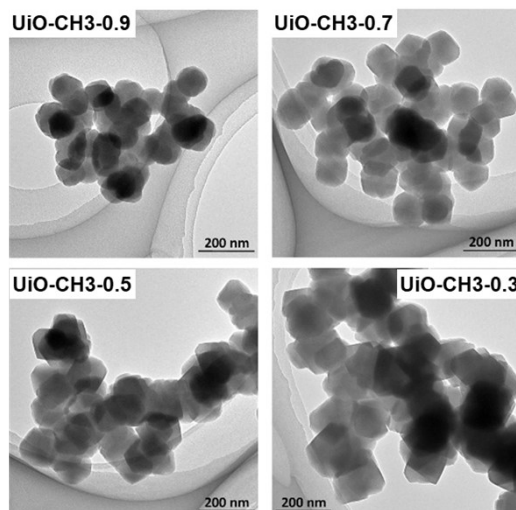
Fig. S5 TEM images of UiO-66-CH$_3$ samples.
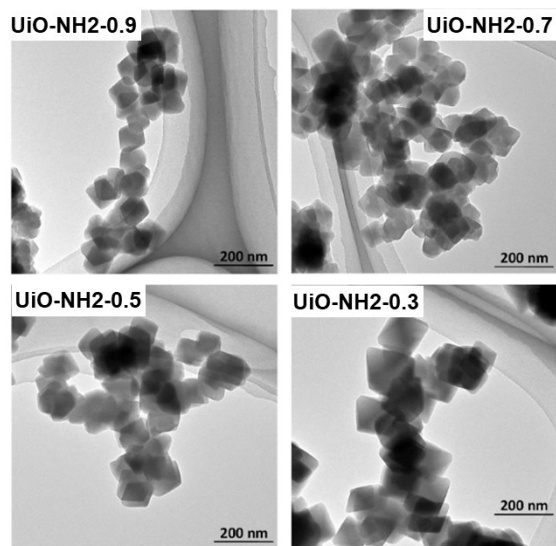
Fig. S6 TEM images of UiO-66-NH$_2$ samples.
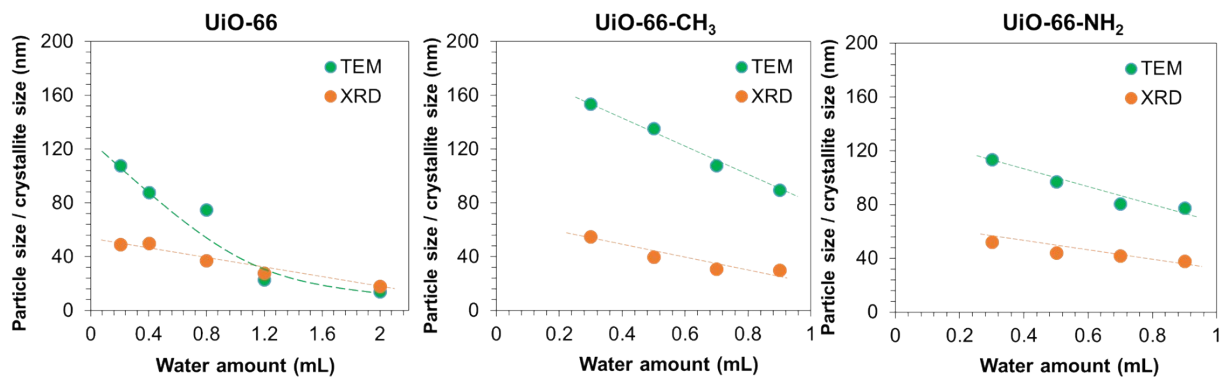
Fig. S7 Particle size of UiO-66, UiO-66-CH$_3$ and UiO-66-NH$_2$ acquired from TEM images compared to the crystallite size acquired from the (111) diffraction peak using the Scherer's equation.

3. Thermogravimetric analysis

The thermogravimetric analysis (TGA) was performed on a Ragaku ThermoPlus EVO II thermal analyzer. A sample was loaded in an aluminum pan, then heated to 200 °C and kept for 2 h to remove water and residual methanol. Thereafter, the temperature was raised to 600 °C at the heating rate of 5 °/min under dry air. The organic content was calculated based on the weight loss in the range of 300-600 °C, where the final residue at 600 °C corresponded to ZrO_2 and the plateau in the range of 250-400 °C corresponded to the chemical formula of $ZrO(CO_2)_2(C_6H_4)$, $ZrO(CO_2)_2(C_7H_6)$ and $ZrO(CO_2)_2(C_6H_5N)$ for UiO-66, UiO-66-CH_3 and UiO-66-NH_2, respectively.
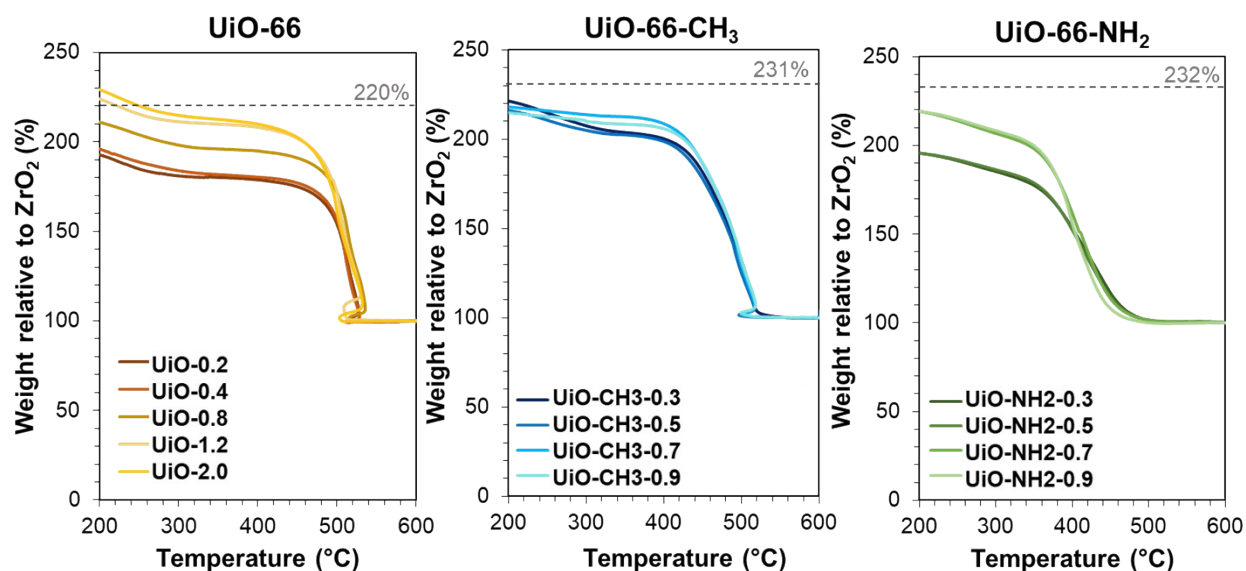
Fig. S8 TGA profiles of UiO-66, UiO-66-CH_3 and UiO-66-NH_2 samples. Y axis is a relative mass loss by setting the final residue as 100%. Dashed lines represent the theoretical values for 12-ligand coordination.

Table S1 Linker:Zr ratios of UiO-66, UiO-66-CH$_3$ and UiO-66-NH$_2$ samples

Sample	Linker:Zr ratio[a]
UiO-0.2	8.5
UiO-0.4	8.7
UiO-0.8	10.0
UiO-1.2	11.2
UiO-2.0	11.5
UiO-CH3-0.3	10.0
UiO-CH3-0.5	9.8
UiO-CH3-0.7	10.5
UiO-CH3-0.9	10.2
UiO-NH2-0.3	8.1
UiO-NH2-0.5	8.2
UiO-NH2-0.7	9.9
UiO-NH2-0.9	10.0

[a]Calculated from the mass loss between 300-600 °C, which ideally attributes to the decomposition of the organic linker from the dehydrated cluster [Zr$_6$O$_6$]$^{12+}$ to form ZrO$_2$ as a final residue.

4. N$_2$ adsorption/desorption measurement

N$_2$ adsorption and desorption isotherms of UiO-66, UiO-66-CH$_3$ and UiO-66-NH$_2$ were acquired at 77 K using a BELSORP-max instrument (BEL JAPAN, Inc.). 20-30 mg of a sample was charged into a sample cell and sealed with a brass filler and a rubber cap. The sample was outgassed at 150 ºC for 24 h *in vacuo* prior to the measurement. The total surface area and the mesoporous surface area were respectively calculated from the Brunauer–Emmett–Teller (BET) and Barrett–Joyner–Halenda (BJH) methods. The microporous surface area was obtained by subtracting the mesoporous surface from the total surface area. The micropore size distribution was calculated using the NLDFT method embedded in the BELMaster7™ software.

Table S2 Surface areas of UiO-66 samples

Sample	BET surface area (m^2 g^{-1})	Mesoporous surface area[a] (m^2 g^{-1})	Microporous surface area[b] (m^2 g^{-1})
UiO-0.2	1119	61	1058
UiO-0.4	1018	84	934
UiO-0.8	1068	83	985
UiO-1.2	798	206	593
UiO-2.0	804	251	553

[a]Calculated from the BJH method for the pore size $\geq$2 nm, [b]calculated by subtracting the BJH surface area from the BET surface area.
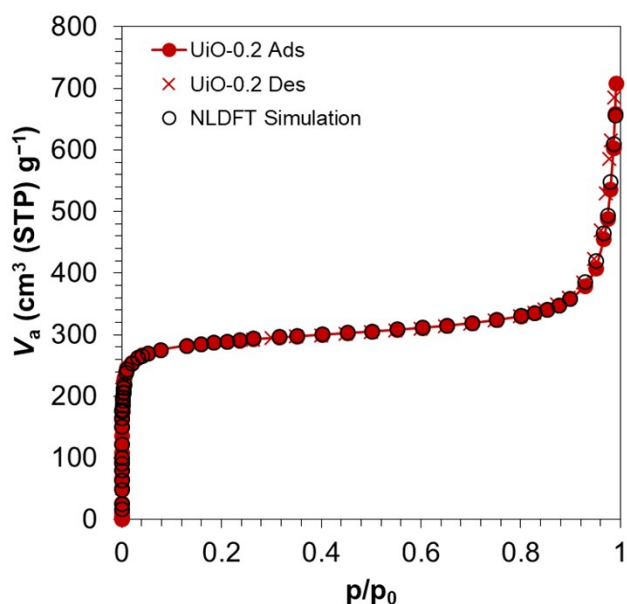
Fig. S9 N$_2$ adsorption/desorption isotherm and the adsorption branch simulated by NLDFT for UiO-0.2.
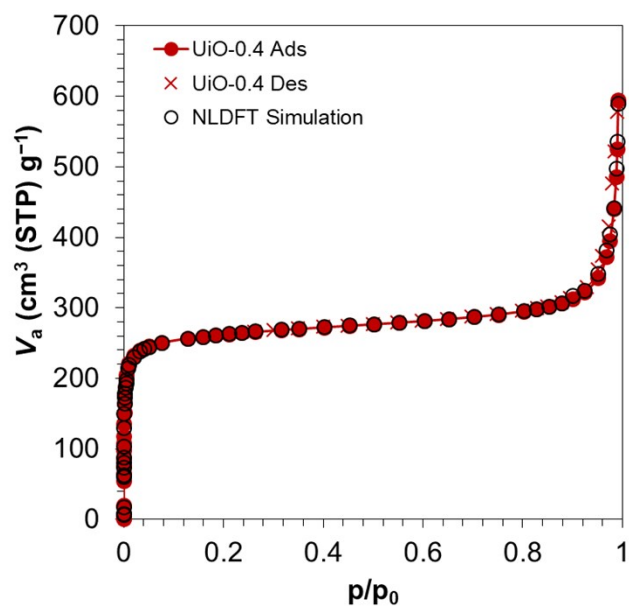
Fig. S10 N_2 adsorption/desorption isotherm and the adsorption branch simulated by NLDFT for UiO-0.4.
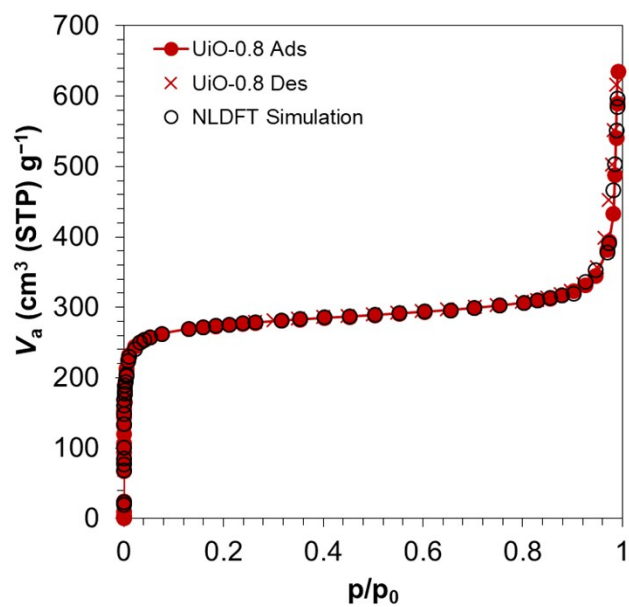
Fig. S11 N_2 adsorption/desorption isotherm and the adsorption branch simulated by NLDFT for UiO-0.8.
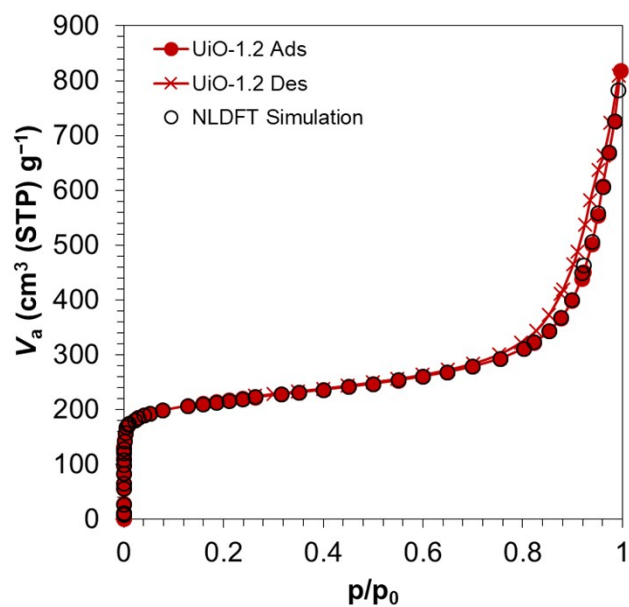
Fig. S12 N_2 adsorption/desorption isotherm and the adsorption branch simulated by NLDFT for UiO-1.2.
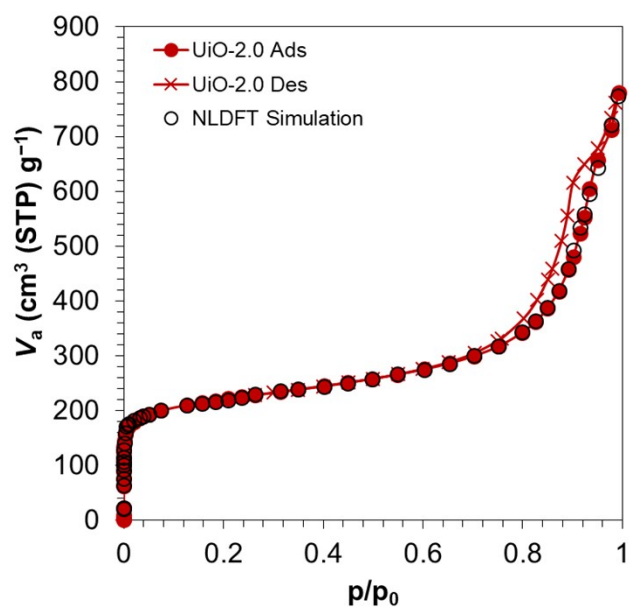
Fig. S13 N_2 adsorption/desorption isotherm and the adsorption branch simulated by NLDFT for UiO-2.0.
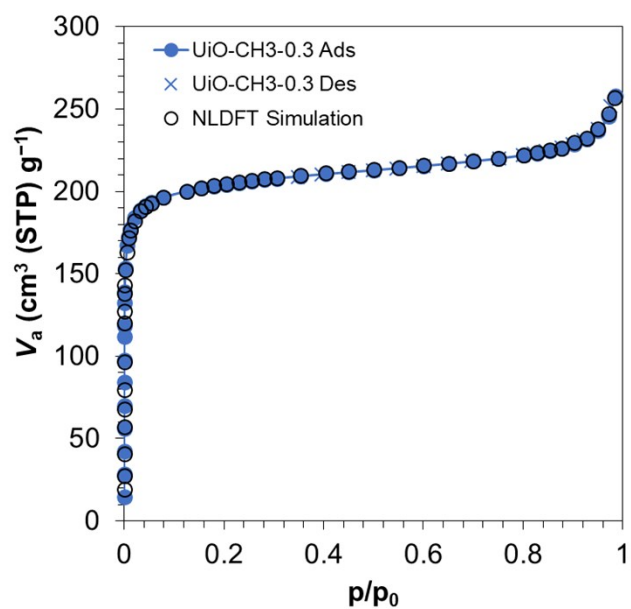
Fig. S14 N$_2$ adsorption/desorption isotherm and the adsorption branch simulated by NLDFT for UiO-CH3-0.3.
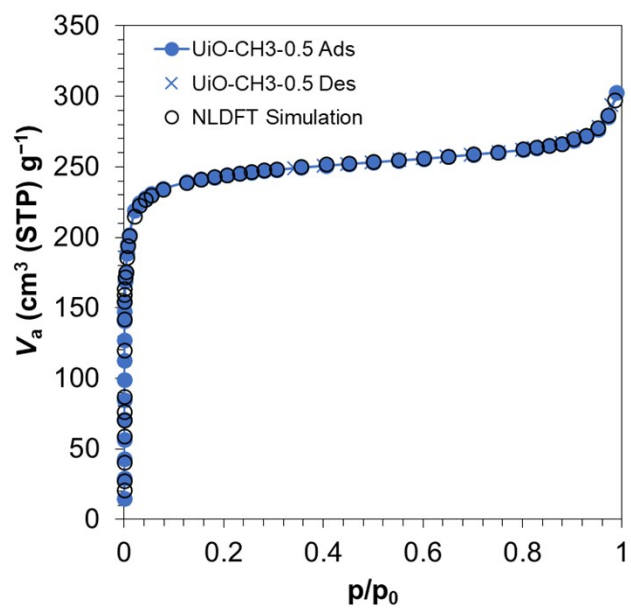
Fig. S15 N$_2$ adsorption/desorption isotherm and the adsorption branch simulated by NLDFT for UiO-CH3-0.5.
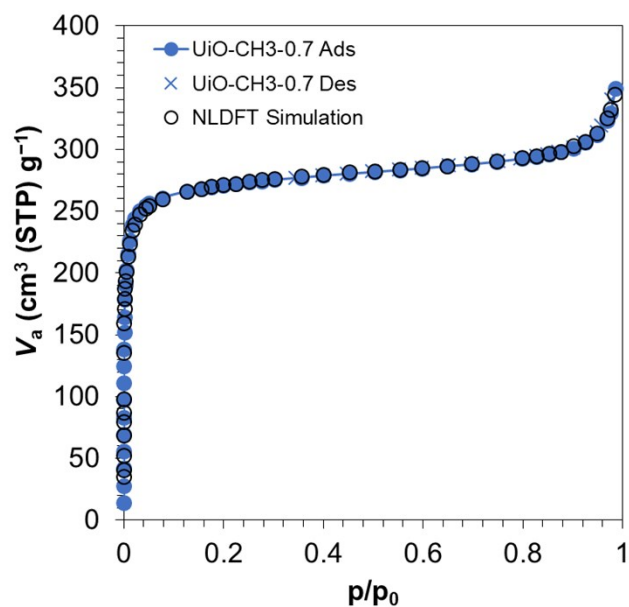
Fig. S16 N$_2$ adsorption/desorption isotherm and the adsorption branch simulated by NLDFT for UiO-CH3-0.7.
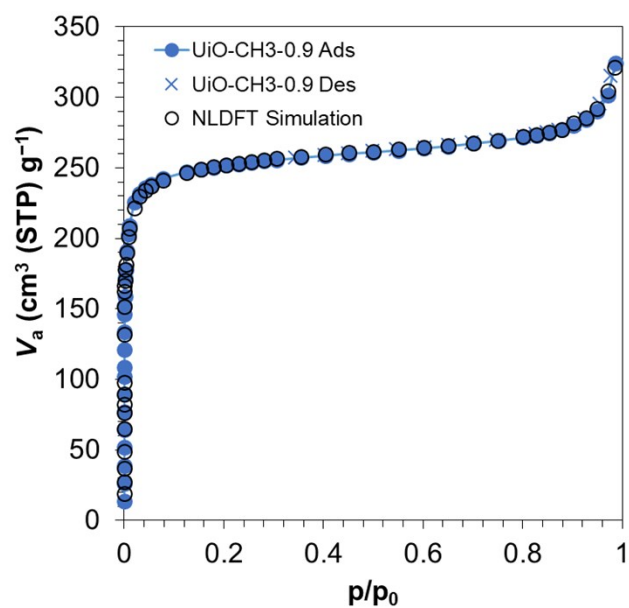
Fig. S17 N$_2$ adsorption/desorption isotherm and the adsorption branch simulated by NLDFT for UiO-CH3-0.9.
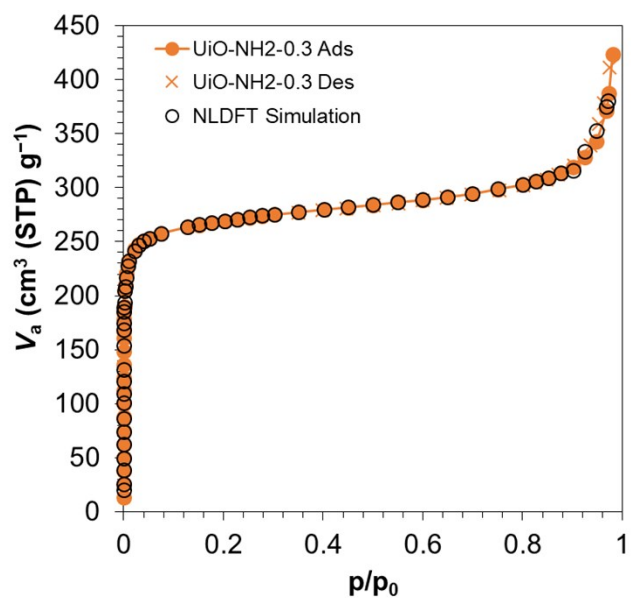
Fig. S18 N$_2$ adsorption/desorption isotherm and the adsorption branch simulated by NLDFT for UiO-NH2-0.3.
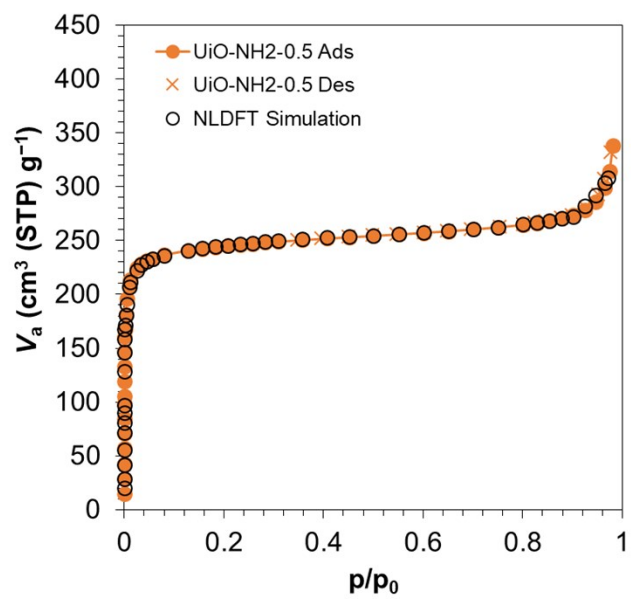
Fig. S19 N$_2$ adsorption/desorption isotherm and the adsorption branch simulated by NLDFT for UiO-NH2-0.5.
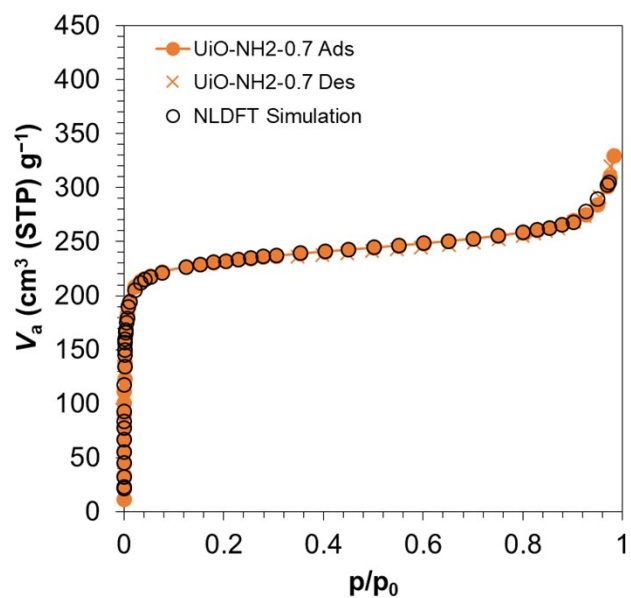
Fig. S20 N$_2$ adsorption/desorption isotherm and the adsorption branch simulated by NLDFT for UiO-NH2-0.7
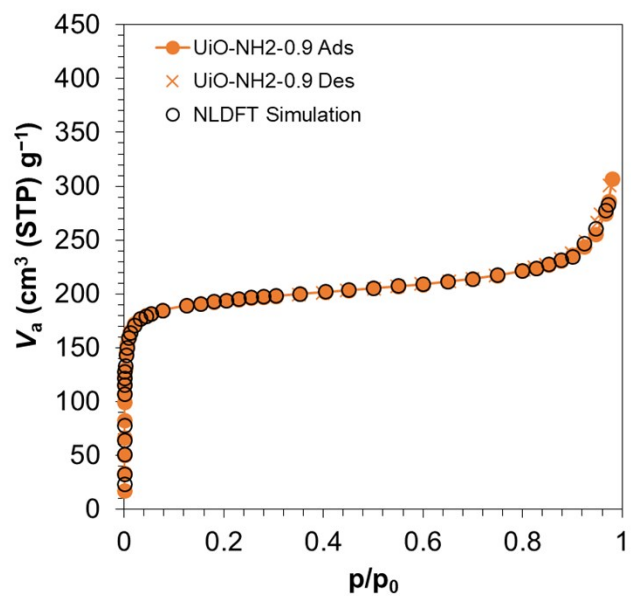
Fig. S21 N$_2$ adsorption/desorption isotherm and the adsorption branch simulated by NLDFT for UiO-NH2-0.9.

5. X-ray photoelectron spectroscopy

X-ray photoelectron spectroscopy (XPS) analysis was performed on a Shimadzu Kratos AXIS Ultra DLD. Photoelectrons were excited by monochromated Al Kα radiation. The X-ray gun was operated at 10 kV and 15 mA. The survey scan was collected from -5 to 1000 eV with the pass energy of 160 eV, followed by the detailed scan at the Cl 2p region with the pass energy of 40 eV, step size of 0.1 eV and 10 accumulated sweeps.
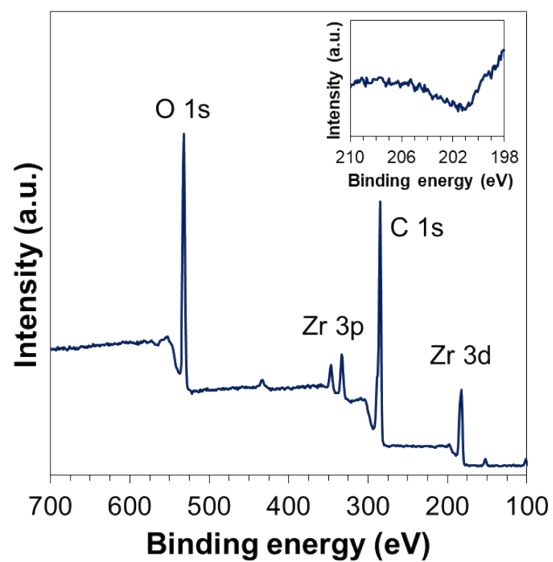
Fig. S22 XPS spectrum of UiO-66 (UiO-0.4). Inset shows the detailed scan at the Cl 2p region.

6. Acid-base titration

20-30 mg of the UiO-66 sample was suspended in 50 mL of a 0.01 M $NaNO_3$ solution, and kept for 24 h under stirring. The pH of the solution was adjusted by a HCl solution to the value of 3.0 prior to the titration with a 0.1 M NaOH solution. The addition rate of the NaOH solution was controlled at 20 μm/min and the pH value was recorded at the interval time of 1 min.
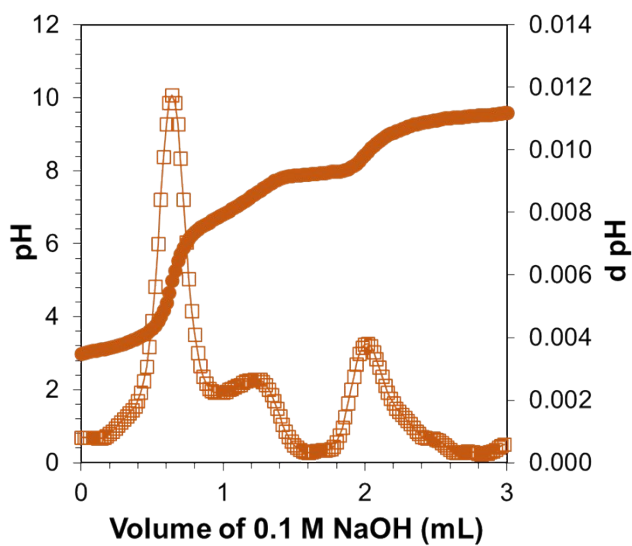
Fig. S23 Acid-base titration curve (filled) and first-derivative curve (unfilled) for UiO-66 (UiO-0.4). The number of protons arising from under-coordinated Zr atoms was calculated as 6.34 mmol H^+ per gram UiO-66.

7. Fourier-transform infrared spectroscopy

Fourier transform infrared spectra (FTIR) of UiO-66 samples were acquired on a Jasco FT/IR-6100 spectrometer in the range of 400-2400 cm^{-1} with a resolution of 4 cm^{-1}. The dried sample was diluted with potassium bromide powder, and then pressed into a pellet for the measurement in the transmission mode.
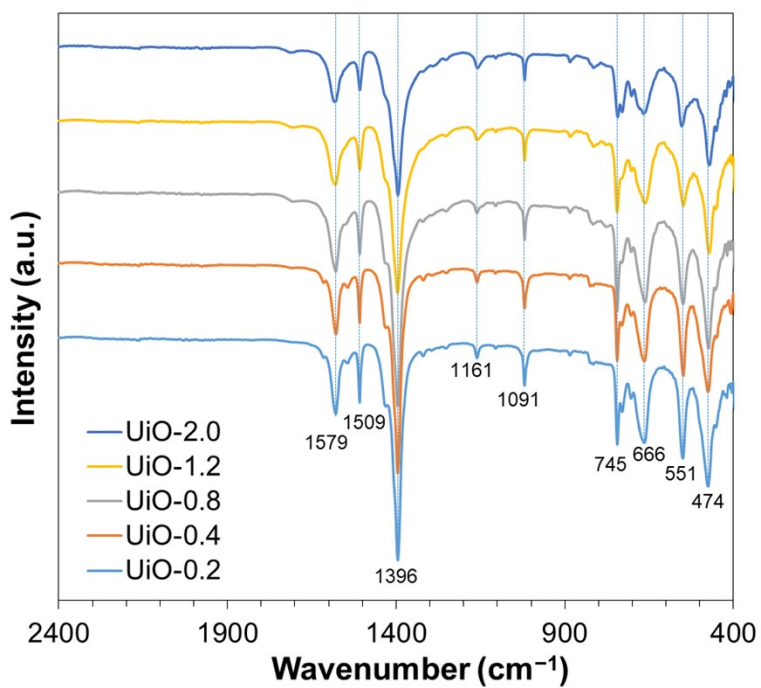
Fig. S24 FTIR spectra of UiO-66 samples.

8. Analysis of reaction products

The analysis of reaction products was done using a gas chramatography (GC, Agilent 7890A) equipped with a flame-ionization detection and a DB-wax UI capillary column (30 m in length and 0.32 mm diameter). The injection temperature was set at 250 °C. The temperature gradient was used as follows: 50 °C for a holding time of 1 min, then increase to 200 °C at the heating rate of 10 °C min^{-1} and hold for 5 min. The split ratio was used at 50:1. The retention times of the reactant and the reaction product from Meerwein-Ponndorf-Verley reduction of 4-*tert*-butylcyclohexanone and alcoholysis of styrene oxide are shown in Fig. S25 and S26, respectively.
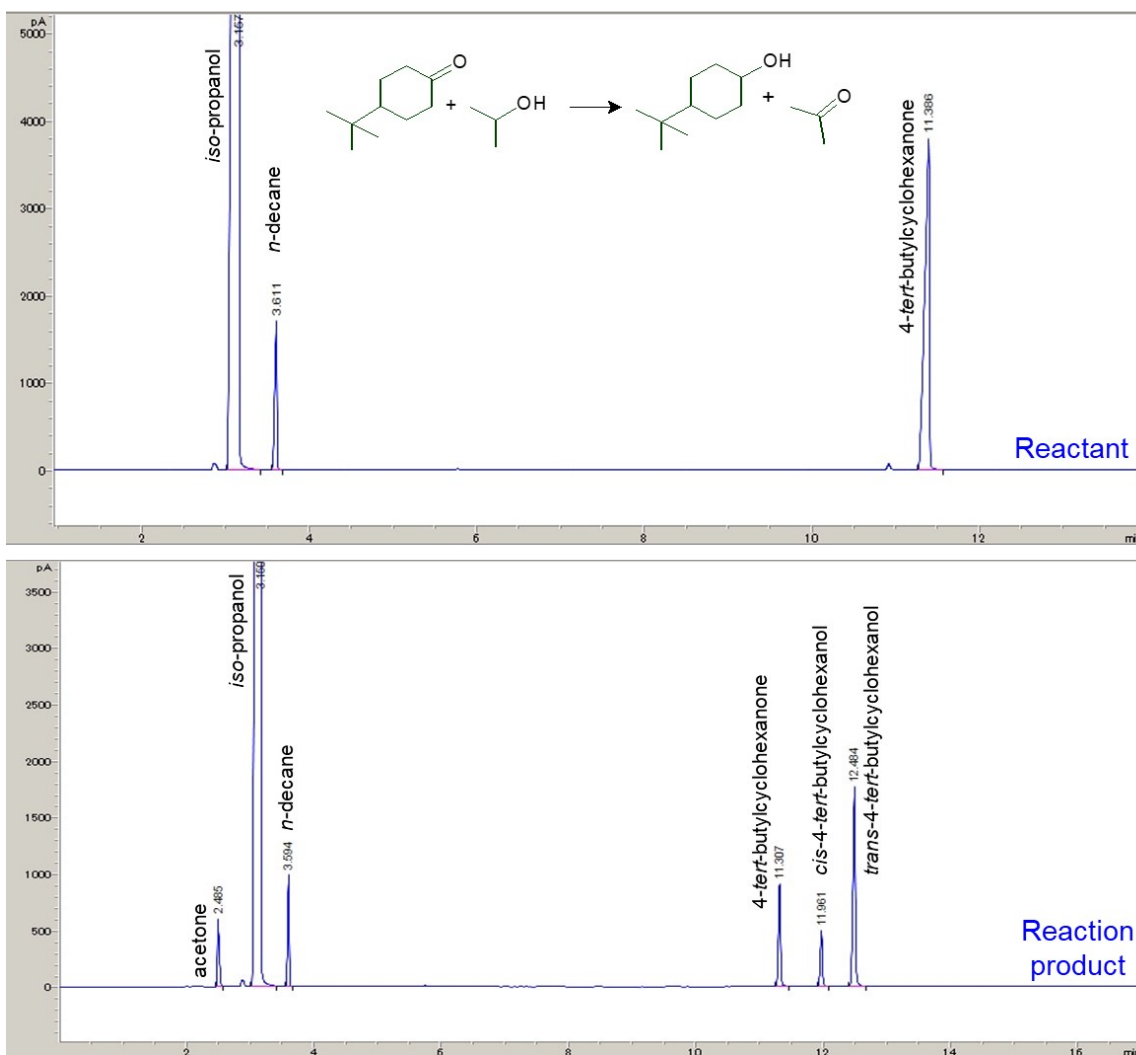
Fig. S25 GC chromatographs of the reactant and reaction product in Meerwein-Ponndorf-Verley reduction of 4-*tert*-butylcyclohexanone.
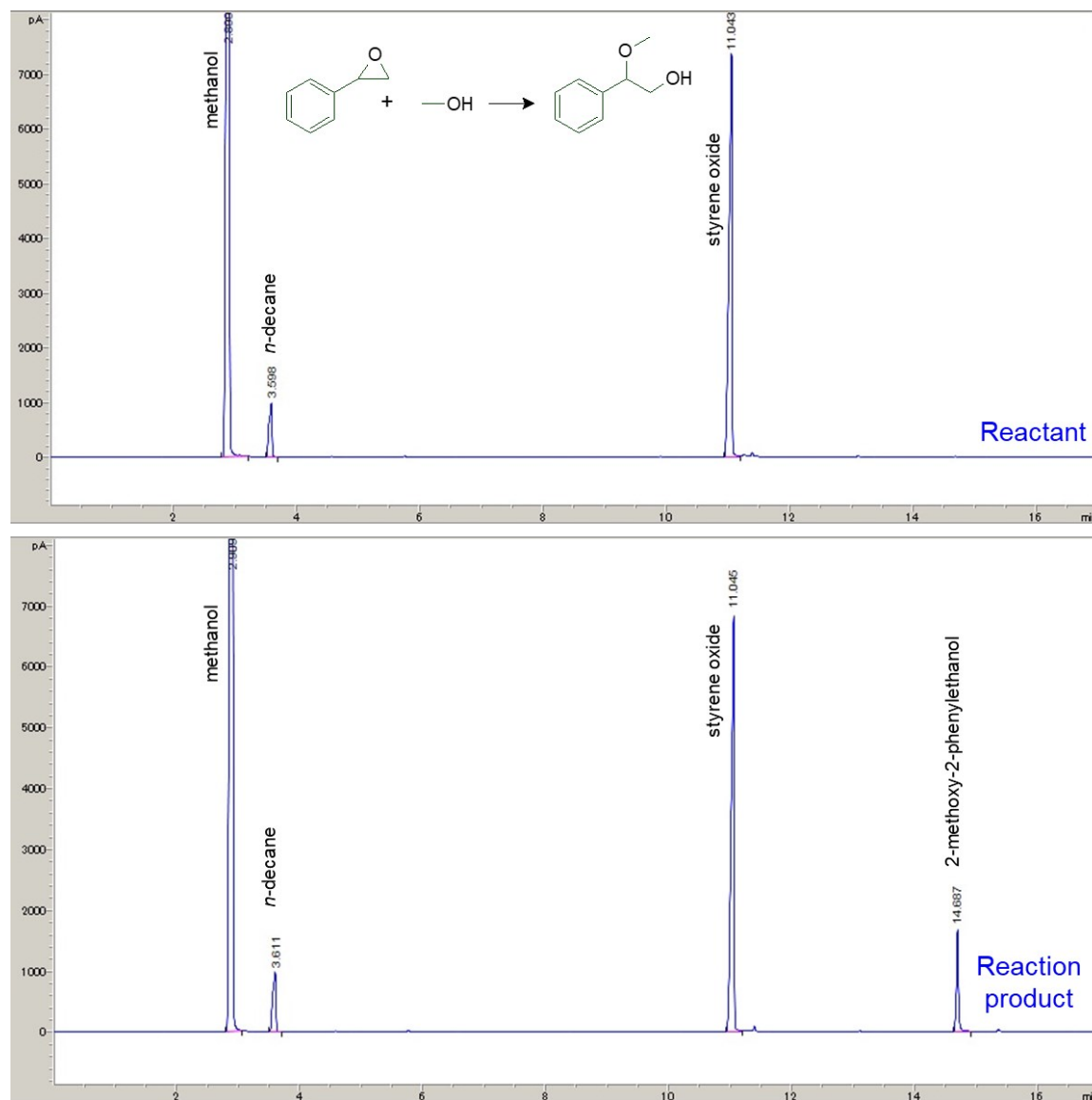
Fig. S26 GC chromatographs of the reactant and reaction product in alcoholysis of styrene oxide.

18

9. Catalyst recyclability and structural retention

The catalyst recyclability and structural retention tested in the MPV reduction of 4-*tert*-butylcyclohexanone. 10 reaction cells containing 4-*tert*-butylcyclohexanone (0.5 mmol), isopropanol (2.0 mL), a catalyst (10 mg), and *n*-decane (20 µL) as an internal standard were heated at 80 °C under stirring for 24 h. After the reaction, the nanoparticles were collected from each cell by centrifugation and combined to get a sufficient amount of nanoparticles. The sample was repetitively washed with methanol for 5 times and dried under vacuum for 2 h before using in the second run. The XRD patterns of UiO-66 (UiO-0.4) after the first and the second runs are shown in Fig. S27.
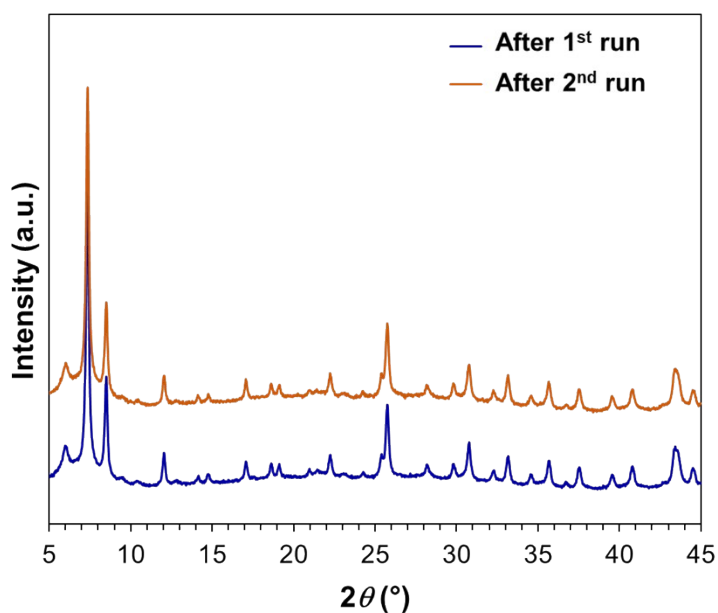
Fig. S27 XRD patterns of UiO-66 (UiO-0.4) after using in the MPV reduction of 4-*tert*-butylcyclohexanone.